RESEARCH ARTICLE | SEPTEMBER 17 2009

Crossover from nucleation to spinodal decomposition in a condensing vapor

Jan Wedekind; Guram Chkonia; Judith Wölk; Reinhard Strey; David Reguera

J. Chem. Phys. 131, 114506 (2009)
https://doi.org/10.1063/1.3204448

Crossover from nucleation to spinodal decomposition in a condensing vapor

Jan Wedekind,[1,a)] Guram Chkonia,[2] Judith Wölk,[2] Reinhard Strey,[2] and David Reguera[1]
[1]*Departament de Física Fonamental, Universitat de Barcelona, Martí i Franquès 1, 08028 Barcelona, Spain*
[2]*Institut für Physikalische Chemie, Universität zu Köln, Luxemburger Str. 116, 50939 Köln, Germany*

(Received 13 May 2009; accepted 22 July 2009; published online 17 September 2009)

The mechanism controlling the initial step of a phase transition has a tremendous influence on the emerging phase. We study the crossover from a purely nucleation-controlled transition toward spinodal decomposition in a condensing Lennard-Jones vapor using molecular dynamics simulations. We analyze both the kinetics and at the same time the thermodynamics by directly reconstructing the free energy of cluster formation. We estimate the location of the spinodal, which lies at much deeper supersaturations than expected. Moreover, the nucleation barriers we find differ only by a constant from the classical nucleation theory predictions and are in very good agreement with semiempirical scaling relations. In the regime from very small barriers to the spinodal, growth controls the rate of the transition but not its nature because the activation barrier has not yet vanished. Finally, we discuss in detail the influence of the chosen reaction coordinate on the interpretation of such simulation results. © *2009 American Institute of Physics*.
[doi:10.1063/1.3204448]

I. INTRODUCTION

Nucleation and spinodal decomposition are two very distinct mechanisms behind phase transitions such as crystallization, condensation, or melting, their occurrence depending on how far a substance is pushed away from the coexistence line. These initial steps of the transition have a tremendous influence on the growth dynamics and final structure of the new bulk phase and it is highly desirable to control and understand the signatures and the crossover between the two to optimize many scientific and industrial processes, such as protein crystallization, solidification of polymer melts, or nanoparticle production. It is therefore no surprise that the topic has received considerable attention in the literature.[1–13]

When a vapor is supersaturated or supercooled beyond the vapor-liquid coexistence line, it enters a *metastable* regime that is characterized by the presence of a free-energy barrier. This nucleation barrier arises because the smallest clusters of the new liquid phase are thermodynamically less favorable than the old bulk vapor phase. In this metastable state, the phase transition can only be triggered through a rare, random, and localized fluctuation forming a sufficiently large liquid embryo that is able to grow on spontaneously. Quenching the system deeper and deeper decreases the nucleation barrier until the point where it vanishes, which is where we locate the *kinetic* spinodal. From this point on, the fluid is *unstable* rather than metastable and the phase transition is no longer controlled by the presence of a free-energy barrier but solely by spinodal decomposition. Intuitively one is inclined to think that this kinetic definition of spinodal should coincide with the *thermodynamic* spinodal, which represents the absolute stability limit of a fluid and is located at the point where the thermodynamic response functions such as the isothermal compressibility or the isobaric heat capacity diverge. In fact, there is a strong evidence that this is the case, at least for the vapor-liquid transition.[14]

In the two limits of a high free-energy barrier or no barrier at all, both processes can be clearly distinguished from each other. On the one hand, the presence of a high barrier leads to a strong separation of the two time scales involved: The long time before the rare occurrence of a spontaneous localized fluctuation triggering nucleation and the short time of subsequent fast growth of this liquid embryo. On the other hand, when no barrier is present any infinitesimally small fluctuation in the density is sufficient to trigger the phase transition, which immediately starts by a collective and diffusive growth of the new phase throughout the entire system. However, it has been suggested that there exists a transition regime for small barriers of the order of $1k_BT$ or less, where both process are thought to be concurrent, often being coined *spinodal nucleation*.[3,4,6] A clear separation of the two contributions obviously would be quite difficult in such a regime.

In this work, we study the crossover from a purely nucleation-controlled process to spinodal decomposition in a condensing Lennard-Jones (LJ) vapor. We employ standard molecular dynamics (MD) simulations to study the kinetics of the process. At the same time and from the same simulation results, we are also able to directly reconstruct the free energy of cluster formation and study the thermodynamics of the process without resorting to biased Monte Carlo (MC) or path-sampling techniques. Our findings underline the importance of carefully interpreting the obtained results and theoretical predictions in the light of the chosen reaction coordinate. Bearing this in mind, we are able to estimate the

[a)]Electronic mail: janw@ffn.ub.es.

location of the spinodal, which seems to lie at much deeper supersaturations than the estimate from the LJ equation of state (EOS). Moreover, the nucleation barriers we find are in very good agreement with semiempirical scaling relations proposed by McGraw and Laaksonen,[15] which suggest that the classical nucleation theory (CNT) prediction is only off by a temperature-dependent constant. Finally, we observe how cluster growth controls the rate of the phase transformation, but not its nature, in the transition regime from very small barriers up to the spinodal.

II. METHODS

A. Simulation details

We have performed standard MD simulations[16,17] of the nucleation of LJ argon. In these simulations, $N=512$ argon atoms are placed in a cubic box with periodic boundary conditions at $T=80.7$ K, corresponding to a reduced temperature of $T^*=0.67$. The time step was 5 fs and the LJ parameters were $\varepsilon_{LJ}/k_B=120$ K and $\sigma_{LJ}=0.3405$ nm. The potential was cut off but unshifted at $6.78\sigma_{LJ}$, which should be sufficiently long range to be comparable to the full LJ. We verified that the small system size, the thermostat, and the time step have no significant influence on the results.[18,19] The metastable properties of the LJ vapor for this particular cutoff and temperature are given in Ref. 20. Clusters of liquid atoms are identified using the ten Wolde–Frenkel cluster definition,[21] which provides an accurate description of liquid clusters,[22] and we sample the cluster-size distribution in the system at regular intervals (1000 time steps or less).

Typically, the supersaturation in vapor-liquid nucleation is given as $S=p/p_{eq}$, where p is the vapor pressure and p_{eq} the equilibrium vapor pressure at T. However, from a careful analysis of the kinetics of nucleation,[23] the more appropriate way of defining supersaturation is the ratio between the actual monomer concentration and the concentration of monomers at saturation. We therefore define the supersaturation as $S\equiv\rho/\rho_{eq}(T)$, i.e., as the ratio of the initial vapor density ρ over the equilibrium (or saturation) density $\rho_{eq}(T)$ given in Ref. 20. This definition of supersaturation coincides with the standard one for an ideal gas.

B. Kinetic analysis: Nucleation rates and critical cluster sizes

The relevant kinetic information about the process was obtained by monitoring the size of the *largest* cluster as reaction coordinate and using the recently developed mean first-passage time (MFPT) analysis. From the full cluster-size distribution we extract the size of the largest cluster n in the system and the time $t_i^{larg}(n)$ at which this largest cluster passes through size n for the first time. The *mean* first-passage time $\tau_{larg}(n)$ for each size n is obtained by averaging $t_i^{larg}(n)$ over R realizations of the simulation with different initial configurations: $\tau_{larg}(n)=\Sigma_i t_i^{larg}(n)/R$. For this purpose we typically performed $R=300$ simulations at each condition. Figure 1 shows the resulting MFPT curves as a function of the largest cluster size for six different values of the supersaturation. We can extract the steady-state nucleation rate J, the critical cluster size n_τ^*, and the Zeldovich factor Z that

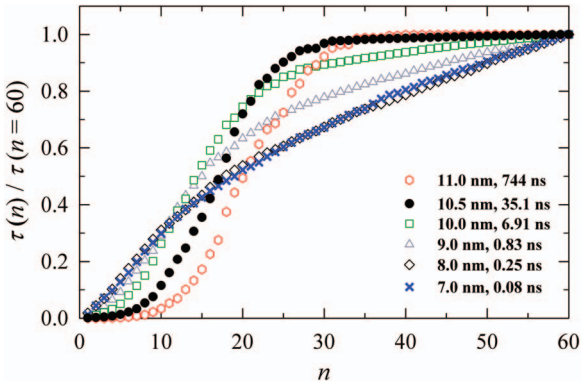

FIG. 1. Mean first-passage time $\tau_{larg}(n)$ of the largest cluster as a function of size n for different supersaturations. For clarity, the data are scaled by the last point $\tau_{larg}(n=60)$, whose value is given in the legend for each supersaturation S.

is related to the local curvature of the free energy of formation around the top of the nucleation barrier by fitting the MFPT to an error function:[24]

$$\tau_{larg}(n)=\frac{\tau_J}{2}[1+\mathrm{erf}(Z\sqrt{\pi}(n-n_\tau^*))]. \quad (1)$$

The nucleation rate then is $J=(\tau_J V)^{-1}$ and the critical cluster size is roughly located at the inflection point of the MFPT curve. This procedure is very accurate as long as the activation barrier is sufficiently high. A good indicator for this is the sigmoidal shape of the MFPT curves reaching a well-defined plateau for postcritical sizes. This plateau signals that it takes a much longer time to form a cluster that has successfully overcome the barrier (roughly at $2n_\tau^*$) than it takes the same cluster to continue to grow on by the same amount (up to $4n_\tau^*$). Figure 1 shows such a plateau in the MFPT for moderately supersaturated systems. For higher supersaturations, no plateau is reached and it becomes increasingly difficult to fit the MPFT curve to Eq. (1) with reasonable results.[25] In these cases, the rate of formation of a cluster strongly depends on its size. Therefore, as a unified estimate of nucleation rate we use the definition

$$J=\frac{1}{\tau(n=60)V}, \quad (2)$$

connected to the time of formation of a large enough postcritical cluster of size $n=60$.[25–27] The same size was used as the absorbing boundary in the reconstruction of the free-energy of formation, as described in Sec. II C.

C. Thermodynamic analysis: Reconstruction of the free energy of cluster formation

Next to the kinetic information that we obtain directly from the MFPT, we were also able to reconstruct the free energy of cluster formation by using a new method introduced in Ref. 28 that requires both the MFPT as well as the steady-state probability distribution. The steady-state probability $P_{larg}^{st}(n)$ is obtained from a histogram of the different values of the size of the largest cluster accumulated in all simulation runs for a given supersaturation, in which we discarded the first 1000 time steps to remove the transient. Us-

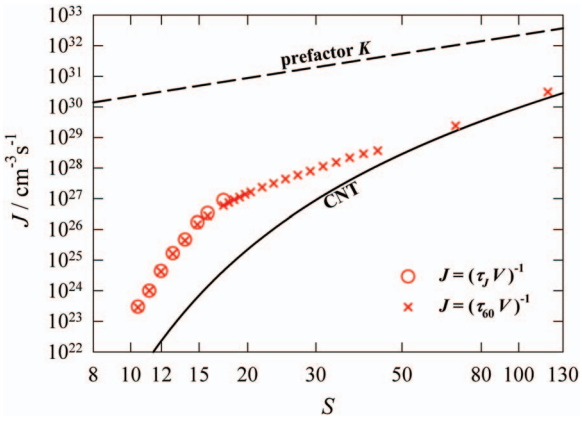

FIG. 2. Nucleation rates J obtained from the MD simulations as a function of the supersaturation S. Circles: fit of the MFPT, Eq. (1). Crosses: $J=[\tau_{\mathrm{larg}}(n=60)\ V]^{-1}$, Eq. (2). Also shown are the predictions by CNT (solid line) and the kinetic prefactor of CNT (dashed line).

ing these two ingredients, we can reconstruct the free energy of formation as indicated in Ref. 28 by calculating first

$$B(n) = -\frac{1}{P^{\mathrm{st}}_{\mathrm{larg}}(n)}\left[\int_n^b P^{\mathrm{st}}_{\mathrm{larg}}(n')dn' - \frac{\tau_{\mathrm{larg}}(b)-\tau_{\mathrm{larg}}(n)}{\tau_{\mathrm{larg}}(b)}\right], \tag{3}$$

where b in this case is an absorbing boundary up to which we sample both $P^{\mathrm{st}}_{\mathrm{larg}}(n)$ and $\tau_{\mathrm{larg}}(n)$, "absorbing" in the sense that once the largest cluster has passed through this boundary in a simulation the following time steps are discarded from the statistics. We chose $b=60$ in our simulations. We then use

$$\beta\Delta G_{\mathrm{larg}}(n) = \beta\Delta G_{\mathrm{larg}}(n_1) + \ln\left(\frac{B(n)}{B(n_1)}\right) - \int_{n_1}^{n}\frac{dn'}{B(n')} \tag{4}$$

to reconstruct the free energy $\Delta G_{\mathrm{larg}}(n)$ for any desired interval $[n_1 \le n \le b]$. Here $\beta=1/k_{\mathrm{B}}T$. The integrals in Eqs. (3) and (4) are evaluated by standard discretization techniques (e.g., Ref. 29). As a reference point we used $n_1=1$ and $\beta\Delta G_{\mathrm{larg}}(n=1)=-\ln P^{\mathrm{st}}_{\mathrm{larg}}(n=1)$. We discuss the choice of this reference point and its influence on the height of the reconstructed barrier in the Appendix.

III. RESULTS

A. Nucleation rates

Figure 2 shows the nucleation rate (red circles and crosses) as a function of the supersaturation on a double-logarithmic scale. The results are also detailed in Table I. As expected, the nucleation rate strongly increases with supersaturation, spanning more than six orders of magnitude. As discussed above, at higher S we are only reporting the rate of formation derived from Eq. (2), since the absence of a clear plateau in the MFPT limits the application of the method based on the fit of Eq. (1) to the MFPT. Note that both rates

TABLE I. Simulation results: box size l, number of particles N, supersaturation S, number of simulation runs R, nucleation rate $J(\tau_J)$ [Eq. (1)], nucleation rate $J(\tau_{60})$ [Eq. (2)], reconstructed barrier heights $\Delta G^*_{\mathrm{larg}}$ and ΔG^*, and the critical sizes obtained from the MFPT, n^*_τ, and the barrier reconstruction (BR), n^*_{BR}.

l (nm)	N	S	R	$J(\tau_J)$ 10^{25} cm^{-3} s^{-1}	$J(\tau_{60})$ 10^{25} cm^{-3} s^{-1}	$\Delta G^*_{\mathrm{larg}}$ $k_{\mathrm{B}}T$	ΔG^* $k_{\mathrm{B}}T$	n^*_τ	n^*_{BR}
11.25	512	10.43	175	0.03	0.03	9.2	15.4	21	21
11.00	512	11.16	200	0.10	0.10	8.0	14.2	20	18
10.75	512	11.96	100	0.44	0.42	6.7	12.9	18	16
10.50	512	12.83	300	1.67	1.63	5.8	12.0	17	15
10.25	512	13.79	200	4.69	4.37	5.0	11.2	16	14
10.00	512	14.85	300	17.0	14.5	4.0	10.2	13	13
9.80	512	15.78	300	33.9	27.9	3.5	9.8	13	10
9.50	512	17.33	300	89.6	60.2	3.0	9.2	11	9
9.40	512	17.88	300		75.1				
9.30	512	18.46	300		92.6				
9.20	512	19.07	300		113				
9.10	512	19.71	300		139				
9.00	512	20.37	300		165				
8.80	512	21.79	300		235				
8.60	512	23.34	300		316				
8.40	512	25.05	300		438				
8.20	512	26.93	300		589				
8.00	512	29.00	300		790				
7.80	512	31.30	300		1140				
7.60	512	33.83	300		1550				
7.40	512	36.65	300		2180				
7.20	512	39.79	300		2920				
7.00	512	43.30	300		3700				
6.00	512	68.78	300		2400				
5.00	512	118.81	300		30800				
13.23	1024	12.83	100	1.97	1.84	5.1	12.1	16	14
22.62	5120	12.83	100	1.86	1.51	3.6	12.2	16	14

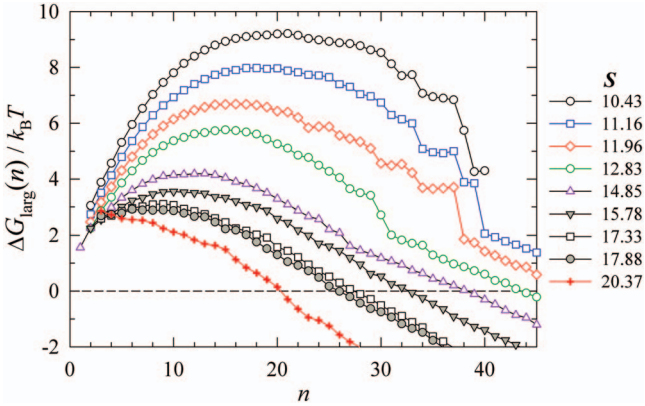

FIG. 3. Free-energy of formation $\Delta G_{\mathrm{larg}}(n)$ for different supersaturations S as a function of the largest cluster size n.

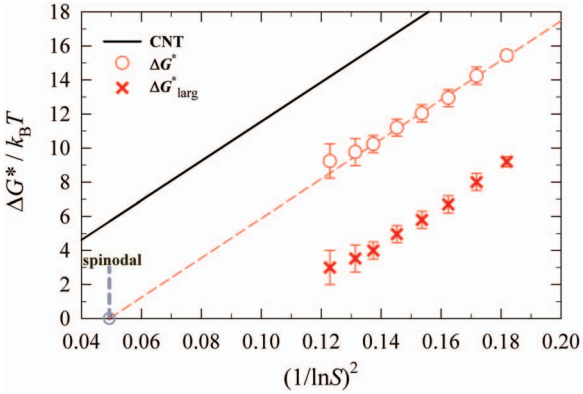

FIG. 4. Height of the nucleation barrier ΔG^* as a function of $(1/\ln S)^2$. Crosses: nucleation barrier $\Delta G^*_{\mathrm{larg}}$ for the largest cluster n directly reconstructed from the MD simulations. Circles: nucleation barrier ΔG^* for any cluster. Solid line: CNT.

are the same in the range where Eq. (1) is still applicable. Also shown is the prediction of CNT (solid black line), where the rate is given by[6]

$$J_{\mathrm{CNT}} = K \exp(-\beta \Delta G^*_{\mathrm{CNT}}), \tag{5}$$

with

$$K = \frac{N}{V} a^* Z = v_l \rho^2 \sqrt{\frac{2\gamma}{\pi m}} \tag{6}$$

being the so-called kinetic prefactor, which depends on the total number of molecules N in the system of volume V, the rate of attachment of individual molecules to the critical cluster $a^* = a(n^*)$, and the Zeldovich factor Z. The height of the nucleation barrier $\Delta G^*_{\mathrm{CNT}}$ is given by

$$\Delta G^*_{\mathrm{CNT}} = \frac{16\pi}{3} \frac{v_l^2 \gamma^3}{(k_{\mathrm{B}} T \ln S)^2}, \tag{7}$$

where v_l is the molar volume in the bulk liquid and γ is the surface tension, which in the absence of better knowledge is commonly taken as the flat bulk surface tension. Both values were taken from Ref. 20.

For small supersaturations, CNT lies almost parallel to the MD result but its prediction is too low by about two orders of magnitude, not an uncommon deviation for CNT. But we already notice that the observed MD rates do not follow the same trend for the higher supersaturations. Later we will see how this relates to growth being the relevant time scale in the system.

B. Free energy of formation and nucleation barriers

Figure 3 highlights some of the individual reconstructed free-energy curves $\Delta G_{\mathrm{larg}}(n)$ as a function of the largest cluster size n. We can clearly see how the barrier height and the critical size, the location of the barrier top, systematically decrease as the supersaturation increases. Toward higher supersaturations, we can observe that the barrier for the largest cluster effectively vanishes, and for even higher supersaturations, the free energy of formation of the largest cluster in the systems goes downhill. Figure 4 shows the height of the nucleation barrier $\Delta G^*_{\mathrm{larg}}$ (crosses) as a function of $(1/\ln S)^2$. Except for the last two points at the highest supersaturations, the data lie on a straight line and the comparison with the CNT prediction from Eq. (7) (solid black line) confirms that CNT overestimates the nucleation barrier height, leading to predictions in the rate that are too low. The deviation in these last two points arises due to the difficulty of locating a "barrier top" of a free-energy curve that is practically flat or almost downhill. These two points therefore represent only a rough estimate.

C. Critical cluster sizes

We determined the critical cluster sizes via three different routes. First, we obtain n^*_τ directly from the fit to the MFPT in Fig. 1 using Eq. (1). Second, we can determine the critical size n^*_{BR} from the location of the top of the reconstructed barrier as shown in Fig. 3. Third, we can make use of the nucleation theorem[30–32] via

$$S \frac{\partial(\beta \Delta G^*_{\mathrm{larg}})}{\partial S} = -n^*_{\mathrm{NT}}, \tag{8}$$

which we determined numerically from the reconstructed barrier heights.

Figure 5 shows the values obtained by the three different methods as a function of $(1/\ln S)^3$, which is the dependency

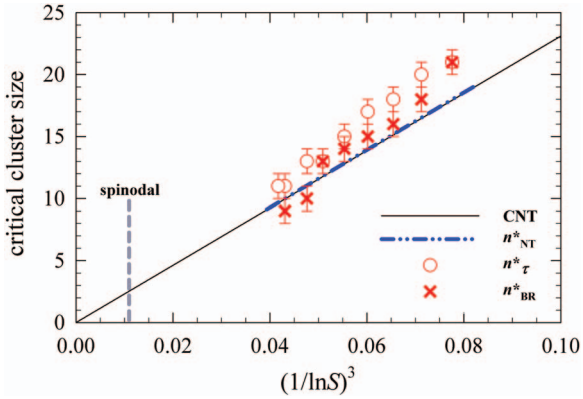

FIG. 5. Critical cluster as a function of $(1/\ln S)^3$. Crosses: critical sizes n^*_{BR} from locating the top of the reconstructed free-energy curve. Circles: fit of the MFPT to Eq. (1), n^*_τ. Solid line: CNT prediction, Eq. (9). Dashed-dotted line: n^*_{BR} from the nucleation theorem, Eq. (8). The gray dashed line marks the location of the spinodal extrapolated from Fig. 4.

predicted by CNT. All three values agree very well with each other, the values n^*_{BR} being slightly smaller than n^*_τ by two atoms or less. This small discrepancy can be due to the discreteness of the size in the reconstruction as well as to the fact that the fit to an error function slightly overestimates the critical cluster size when the nucleation barrier is low. Also shown in Fig. 5 is the prediction of CNT,

$$n^*_{\mathrm{CNT}} = \frac{32\pi}{3}\frac{v_l^2\gamma^3}{(k_{\mathrm{B}}T\ln S)^3}, \tag{9}$$

which shows a good agreement with the MD data. In particular, we note the nearly perfect agreement with the values obtained from the nucleation theorem, which is of particular importance since the critical size obtained from it is independent of the cluster definition.[22]

IV. DISCUSSION

A. Vanishing barrier and the spinodal: Reaction coordinate matters

Figure 4 shows how the barrier $\Delta G^*_{\mathrm{larg}}$ for the largest cluster vanishes for comparatively moderate supersaturations around $S=22$. This result is qualitatively similar to the results presented by Wang *et al.*,[33] Mendez-Villuendas *et al.*,[34] or Bhimalapuram *et al.*[11] Naturally, it raises the question of whether or not we have in fact encountered the spinodal. The clear answer is no. The vanishing of the barrier at this value of S is strongly connected to the choice of the reaction coordinate. From the simulation point of view, it is very convenient to use the size of the largest cluster in the system as the reaction coordinate. However, the true underlying free-energy barrier of interest in nucleation is not the one of the largest cluster, $\Delta G^*_{\mathrm{larg}}$, but the one that *any individual* n-sized cluster in the system has to surmount, ΔG^*. Luckily, both quantities can be related to each other.

The standard description of the kinetics of nucleation, carried out in terms of the free energy of formation of any individual cluster $\Delta G(n)$, leads to an expression of the nucleation rate given by

$$J = \frac{N}{V}a^*Z\exp(-\beta\Delta G^*). \tag{10}$$

If, alternatively, we describe the kinetics of the process using the size of the largest cluster in the systems as a reaction coordinate, the nucleation rate will be given by

$$J = \frac{1}{V}a(n^*)Z\exp(-\beta\Delta G^*_{\mathrm{larg}}) \tag{11}$$

since we only care now about the formation of *one* (the largest) cluster in the system. By making the reasonable assumption that the Zeldovich factor and rate of attachment of molecules to the critical cluster are the same for both any and the largest clusters, one can easily see that $\Delta G^*_{\mathrm{larg}}$ and ΔG^* are connected as

$$\beta\Delta G^* = \beta\Delta G^*_{\mathrm{larg}} + \ln N. \tag{12}$$

Figure 4 shows ΔG^* calculated from this relation, which shifts the true barrier height by the constant value $\ln N$. Thus at the point where $\Delta G^*_{\mathrm{larg}}$ vanishes, the formation of *individual* clusters still is subject to a free-energy barrier of about $\Delta G^* \approx 6k_{\mathrm{B}}T$ in the case where $N=512$.

It should be easy to verify that Eq. (12) is correct by changing the system size, keeping the supersaturation constant. At a fixed S but a different system size, we would expect that $\tau_{\mathrm{larg}}(n)$, $P^{\mathrm{st}}_{\mathrm{larg}}(n)$, and $\Delta G^*_{\mathrm{larg}}$ change considerably while both ΔG^* and the rate J should remain practically constant. We therefore repeated the simulations for a supersaturation $S=12.8$ using two larger system sizes of $N=1024$ and $N=5120$, i.e., systems two and ten times larger. As shown in the Appendix, the result is just as expected: $\Delta G^*_{\mathrm{larg}}$ is lower for $N=512$ by about $\ln(1024/512)\sim 0.7k_{\mathrm{B}}T$ and $\ln(5120/512)\sim 2.3k_{\mathrm{B}}T$ for $N=1024$ and $N=5120$, respectively, but both the nucleation rate J and the true barrier height ΔG^* remain practically unchanged.

This also allows us to answer whether or not the vanishing of $\Delta G^*_{\mathrm{larg}}$ has any special physical significance for the phase transition, e.g., as a limit of thermodynamical stability of the metastable phase.[34] This is not the case since, as we have just shown, the vanishing of $\Delta G^*_{\mathrm{larg}}$ is strongly system size dependent. To further illustrate this point, consider the expected equilibrium Boltzmann distribution $N(n)$ of clusters of size n in the system,[6]

$$N(n) = Ne^{-\beta\Delta G(n)}, \tag{13}$$

and let us determine the barrier for finding exactly one critically sized cluster in the system, i.e., $N(n^*)\equiv 1$. From this condition we immediately find that

$$\ln N \approx \beta\Delta G^* \tag{14}$$

and thus from Eq. (12) that $\Delta G^*_{\mathrm{larg}}=0$.

In other words, the vanishing barrier for the largest cluster only signals the probability that there is already *one* cluster of critical size in the system in the locally equilibrated metastable phase. This critically sized cluster will presumably be the largest in the system and will not feel the presence of the underlying free-energy barrier since it is already on top of it. But this does not mean that the whole metastable phase has suddenly become thermodynamically unstable. It just indicates that the system cannot be kept metastable for long times. On average, the expected rate of formation of clusters of the stable liquid phase, which is still controlled by nucleation mechanism, is such that at least one cluster can form in the system almost right away. A similar explanation has also been considered by Wang *et al.*, who already speculated that the vanishing of the barrier for the largest cluster could not correspond to the spinodal.[33] It is also clear from this discussion that the vanishing of the barrier observed by Bhimalapuram *et al.*[11] does not correspond to the occurrence of a spinodal, as already pointed out by Maibaum.[12,13]

The condition in Eq. (14) is extensive: For larger system sizes N the barrier for the largest cluster will vanish at even higher values of ΔG^*, i.e., even further away from the true spinodal. This pushes to show that, for the practical purpose of gaining as much insight as possible into the nucleation process, it is highly advisable to use a system as small as possible (but not smaller[18]), especially since the size of the largest cluster often is the only feasible and reasonable reac-

tion coordinate we may choose in a simulation. For instance, in a bulk system containing roughly $N=10^{23}$ molecules, Eqs. (13) and (14) then tell us that even for a barrier of about $\ln(10^{23}) \sim 53 k_B T$ there will be at least one critically sized cluster in the system right from the start purely from thermal fluctuations. Therefore, even a system experiencing such apparently high activation barriers for the formation of individual clusters cannot be kept metastable longer than it takes droplets to grow to macroscopical sizes and thus considerably deplete the vapor phase.

We can say that the vanishing of the barrier for the largest cluster signals the conditions at which the metastable mother phase has reached a kinetic limit in the sense that nothing prevents the phase transformation to start right away via the formation and growth of a postcritical cluster. But at these conditions the mother phase is still far from being *mechanically* unstable, in the sense of the *thermodynamic* spinodal. It is worth to remark that the time we can keep a phase metastable (in the sense of preventing the start of the phase transformation) depends on system size and can be estimated from the nucleation rate. Naively, this time can be estimated as $\tau_{\text{metastable}}=1/JV$, which corresponds to the time of formation of at least one critical liquid cluster (i.e., the largest) in the system. Of course, this estimate is smaller than the time required to see a noticeable change in the properties of the mother phase, which depends on how long it takes the largest cluster and the ones that will subsequently appear to grow and eat up a significant fraction of the vapor phase.

It has now become clear that the location of the thermodynamic spinodal is not indicated by the vanishing of the barrier for the largest cluster, ΔG^*_{larg} in the system, but rather the vanishing of the barrier for any individual cluster, $\Delta G^*=0$.

B. Scaling relations hold even for small barriers

The comparison of the reconstructed nucleation barrier with the prediction of CNT in Fig. 4 contains another important aspect: CNT appears to be shifted only by a constant. In addition, Fig. 5 shows that the critical size predicted by CNT agrees quite well with the ones obtained from the simulations. Both conditions correspond to the semiempirical scaling relations proposed by McGraw and Laaksonen,[15] given as

$$\Delta G^* = \Delta G^*_{\text{CNT}} - D(T), \tag{15}$$

$$n^* = n^*_{\text{CNT}}. \tag{16}$$

The surprising feature is that these scaling relations seem to hold down to absolute barriers of only $8k_BT$ and critical cluster sizes of less than ten atoms. In principle, one would have suspected that such simple scaling relations would rather hold at much higher barriers, a regime where the CNT ansatz is more likely to be correct. But our results indicate that this ansatz seems to work quite well even at much lower barriers than anticipated. In addition, the constant offset in the barriers suggest that the origin of the misprediction of CNT cannot be simply attributed to a strong cluster-size dependence of the surface tension since the slope seems to be correct despite the fact that the critical cluster size changes by a factor of 2 along the line. The origin of this discrepancy therefore must also be found in another factor unaccounted for in CNT.

C. Locating the spinodal and comparison with the EOS

Unfortunately, we cannot directly reconstruct the vanishing of the true barrier ΔG^* due to the limitation of monitoring the largest cluster in the simulation. But we are able to pinpoint the location of the spinodal by a simple extrapolation of our results. Trudu *et al.* followed a similar route in their study of freezing,[9] with two main differences: Our results show smaller error and scatter in the determined barrier heights and reach down to even smaller barrier heights closer to the spinodal. Moreover, the quasiperfect scaling revealed in Fig. 4 gives confidence that a simple linear extrapolation in that plot can give us a reasonable estimate of the location of the spinodal.

The extrapolation locates the complete vanishing of the nucleation barrier at a supersaturation of $S_{\text{spin}} \approx 90.3$. We can compare this value with the value obtained theoretically from the LJ EOS (Ref. 35) (including the small corrections due to the truncation of the potential[36]), which yields a value of $S^{\text{EOS}}_{\text{spin}}=32$. The result seems to indicate that the actual thermodynamical stability of the vapor phase extends longer than predicted by the LJ EOS.

But we note that the actual location of the spinodal is quite sensitive to an accurate knowledge of the pressure and density at saturation. Unfortunately, the EOS for the full LJ potential does not quite reproduce the values reported by Baidakov *et al.* for the exact potential we use in this work. Note also that we discard the last two points in this extrapolation because of the difficulties in determining the barrier top (compare Sec. III B). Still, including these points in the extrapolation would lead to an even bigger deviation from the EOS.

D. Critical cluster size: No mean-field divergence

In CNT, the critical cluster size is decreasing as a function of supersaturation. On the other hand, mean-field theory predicts that the critical size should diverge at the spinodal.[4,8] This suggests that, contrary to CNT, n^* should increase upon approaching the spinodal. However, our results give no indication to such a behavior, even though the accessible range goes down to clusters sizes smaller than ten atoms and a barrier height of just about $8k_BT$.

When we extrapolate the critical cluster size n^*_{BR} in Fig. 5 toward higher supersaturations, we find that the critical size at the spinodal S_{spin} would be on the order of 1–2 atoms, while the extrapolation of n^*_τ gives slightly larger values, around 4–5. Physically, a critical size of about 1 would be appealing. It suggests that, in accordance with the decreasing barrier, the critical size also decreases until the point where any liquid monomer already constitutes a successfully nucleated cluster.

In order to gain further insight into the mechanism that controls the phase transition at such extreme supersatura-

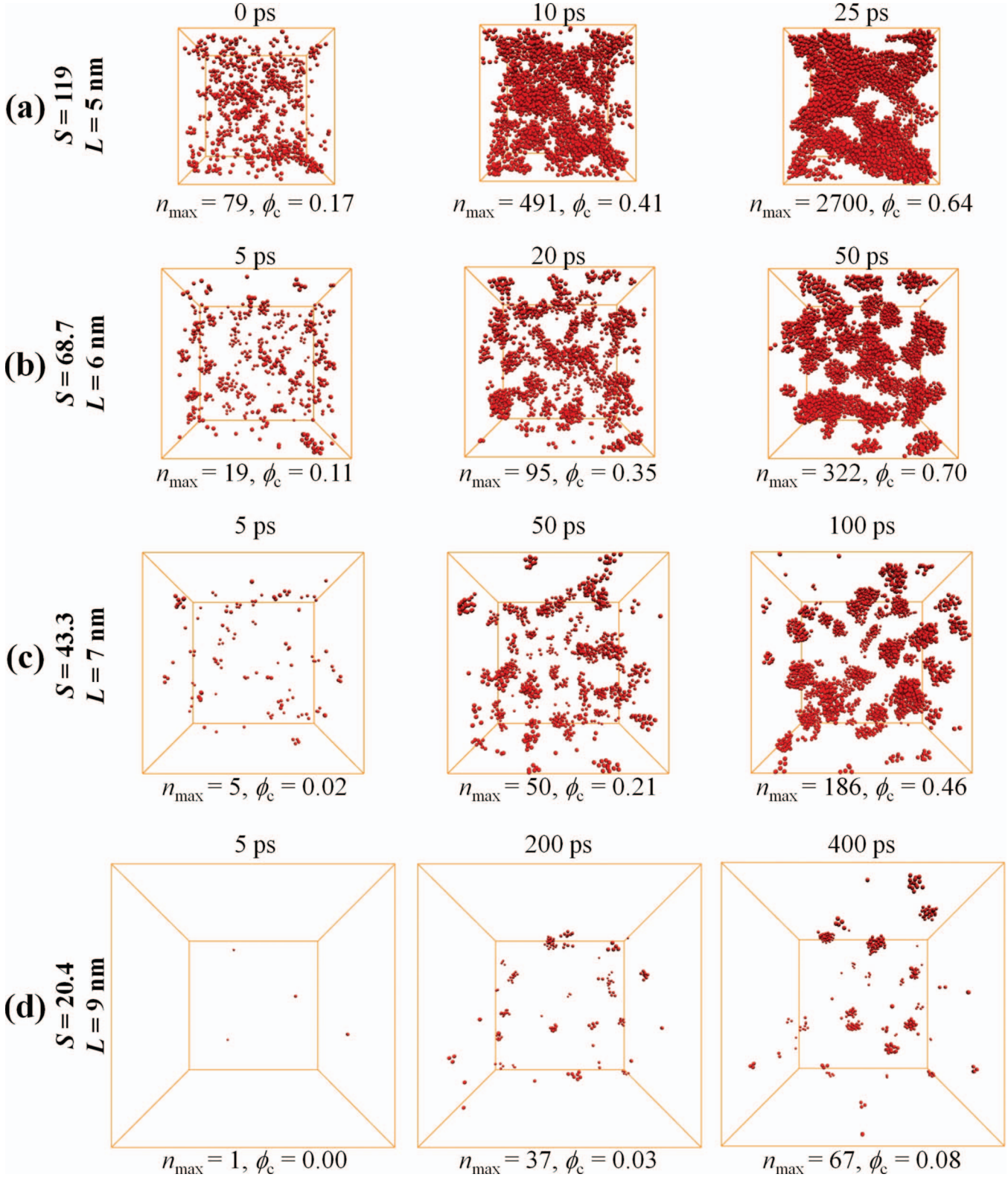

FIG. 6. Snapshots (movies available online) of the time evolution of the phase transition at four different supersaturations $S=20.4$, 43.3, 68.7, and 119 for a system of $N=5120$. Note that all these systems are already beyond the point where the barrier for the largest vanishes. For each snapshot the current size n_{max} of the largest cluster in the system and the total fraction of condensed liquid $\phi_c=\Sigma nN(n)/N$, where $N(n)$ is the number of cluster of size n at the given time, as indicated (enhanced online).[URL: http://dx.doi.org/10.1063/1.3204448.1][URL: http://dx.doi.org/10.1063/1.3204448.2][URL: http://dx.doi.org/10.1063/1.3204448.3][URL: http://dx.doi.org/10.1063/1.3204448.4]

tions, we performed a visual inspection of the time evolution of our simulations at different values of the supersaturation, as shown in Fig. 6 (videos available online). In these snapshots, large red atoms represent only those atoms identified as liquidlike by the ten-Wolde–Frenkel cluster definition we employed. For example, Fig. 6(d) shows three snapshots of one simulation at $S=20.4$, which is actually beyond the conditions where the free energy of the largest vanishes. One can

clearly see that at these conditions, the nucleation mechanism still prevails in the sense that individual, "quasispherical" clusters emerge independently and randomly. This further corroborates that the vanishing of the free energy for the largest cluster does not signal the transition between nucleation and spinodal decomposition.

Figures 6(b) and 6(c) illustrate the evolution of the system closer to the estimated spinodal, where we expect the barrier to be on the order of $2k_BT$ or less. Klein and coworkers suggested that critical clusters close to the spinodal are anisotropic, ramified structures.[10,33] They also observed that at deeper and deeper quenches, this anisotropic character of the nucleation droplets increases significantly. We do not find any significant evidence of elongated, ramified structures or branched fractal clusters. Instead, the phase transformation still seems to proceed by the nucleation of individual quasispherical clusters, even though we are very close to the spinodal. Evidently, it is impossible to obtain a perfectly spherical structure from an object built out of ten or less discrete atoms. Still, when averaged over a sufficient time and/or snapshots at the same size, the average shape still appears to be roughly spherical. However, the same clusters look much more like strongly ramified structures if we use a more connectivity-related cluster criterion in our simulations such as the simple Stillinger cluster definition, which is not as good as the ten-Wolde–Frenkel definition in identifying the true liquidlike clusters.[22]

We also took snapshots of a system at a supersaturation beyond the spinodal at $S=119$ [Fig. 6(a)]. The difference in the mechanism of the transition is striking. The transition immediately proceeds in a collective fashion with large liquid domains branching out through the entire system—a clear signature of spinodal decomposition.

E. Putting the pieces back together: CNT ansatz and Talanquer correction to CNT work well

We have shown that CNT is not able to reproduce the observed nucleation rates, mainly due to an offset in the nucleation barrier of about $6k_BT$. But it is interesting to check whether using the barrier heights ΔG^* reconstructed from the simulations together with the kinetic prefactor of CNT one recovers the measured nucleation rate. We therefore calculated the rate from the barrier reconstruction (BR) according to

$$J_{\mathrm{BR}} = K \exp(-\beta \Delta G^*) \tag{17}$$

and plotted the result in Fig. 7. The rates are in excellent agreement with the measured ones in the range where we could reconstruct the barrier, confirming that the prefactor of CNT is a good approximation and that the basic CNT ansatz works perfectly fine even up to these comparatively small barriers.

Talanquer observed that it should be possible to correct CNT based on the scaling relations of McGraw and Laaksonen from the knowledge of the spinodal alone.[37] The constant in Eq. (15) only depends on temperature but not on supersaturation. If we know the location of spinodal S_{spin} at any given temperature, we can immediately infer that the $D(T)$ in Eq. (15) is given by

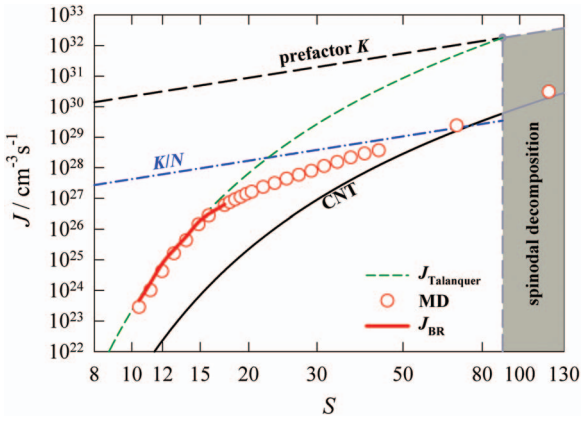

FIG. 7. Nucleation rates as a function of supersaturation (circles). The gray shaded area marks the region of spinodal decomposition. The thick solid line is the nucleation rate calculated from the CNT ansatz J_{BR}, Eq. (17), using the reconstructed barrier heights. The short-dashed line is the rate calculated from the Talanquer correction $J_{\mathrm{Talanquer}}$ using the value of the CNT barrier at the estimated spinodal, Eq. (19). Black solid line: CNT. Long-dashed black line and dashed-dotted line: CNT prefactor K and K/N. For clarity, only the MD rates obtained via Eq. (2) are shown here (circles).

$$D(T) = \Delta G^*_{\mathrm{CNT}}(S_{\mathrm{spin}}). \tag{18}$$

We therefore checked whether CNT corrected by this value,

$$J_{\mathrm{Talanquer}} = K \exp[-\beta(\Delta G^*_{\mathrm{CNT}} - \Delta G^*_{\mathrm{CNT}}(S_{\mathrm{spin}}))], \tag{19}$$

is able to reproduce the nucleation rates in the simulation. The result is also given in Fig. 7. In the same range of values of S as above, the agreement is quite remarkable considering that we could only estimate the location of the spinodal from an extrapolation.

F. Growth-limited kinetics in the transition regime: You cannot walk faster than run

Still, Figs. 2 and 7 contain another important piece of information, one that, in particular, would not be accessible from equilibrium simulations. Equations (17) and (19) both show good agreement with the measured nucleation rate up to moderate supersaturations around $S=15$. But beyond this point the estimated nucleation rate tends to smaller values than predicted by a simple activated approach. This approach tacitly assumes that the time to form a critically sized cluster is much larger than the time it takes to grow to larger sizes. This is no longer a good assumption as we increase the supersaturation. Eventually, at very high supersaturations the time to grow to a large postcritical size is of the same order of magnitude as the time required to overcome the barrier. Therefore, the barrier, which is still present in the system is no longer the rate limiting factor in the phase transition. In terms of the free-energy barrier the system could very quickly form at least one droplet of critical size. But this cluster still needs time to actually grow to a big enough postcritical size through the attachment of molecules. This growth now gradually becomes the rate limiting step of the phase transition and leads to the observed drop in the rates.

A clear indication of this kinetically controlled, growth-limited regime can be found in Fig. 1, where we can see that

at high supersaturations the MFPT follows a universal curve that fits reasonable well with the prediction $\tau(n) \sim n^{2/3}$ of the diffusion-limited growth model.[38]

A simple estimate of the time scale associated with cluster growth is given by K/N, which would be the approximate prediction for the rate following Eq. (11) after the barrier for the largest has vanished. This line is also plotted in Fig. 2. The transition from barrier-dominated to growth-limited rates occurs roughly at the point where $\Delta G^*_{\mathrm{larg}}$ vanishes. Since the vanishing of $\Delta G^*_{\mathrm{larg}}$ depends on the system size, the transition to growth-limited nucleation does too. This transition is just an indication of the conditions at which the appearance of large enough liquid clusters is dictated by the finite time they take to reach that size by the sequential addition of individual atoms. Toward higher supersaturations the measured rates are obviously higher than K/N since the true free energy of formation for the largest rather arguably is downhill rather than flat as tacitly assumed in our crude estimate.

Since we are looking at the MFPT of the largest, our estimates for the rate beyond the vanishing of the free-energy barrier for the largest are limited by the time of growth. But we can still make an estimate of the actual rate at which critical clusters are forming in the system using a method based on the survival probability, as described in Ref. 25. In this method we essentially monitor the probability that any given system has not yet nucleated any cluster of size n_t after a time t. We then fitted the survival probability to the following expression:

$$P_{\mathrm{surv}}(t) = \exp\left(-\frac{t-t_0}{\tau_J}\right), \tag{20}$$

where τ_J controls the actual rate of formation of clusters, whereas t_0 is an estimate of how long it takes for them to grow up to a particular size n_t. Therefore, we can distinguish the rates connected to these two different time scales.

Using this method of analysis and $n_t=60$, we obtain $\tau_J \geqslant t_0$ and the same nucleation rates as with the MFPT at low supersaturations. Remarkably, at the supersaturation where the barrier for the largest vanishes, we find approximately that $\tau_J=t_0$. Moreover, at higher supersaturation we find that τ_J is smaller than t_0. One would naively expect that even though clusters take a time t_0 to grow, the actual nucleation rate given by $1/V\tau_J$ would be larger (eventually by a factor of N close to the spinodal), since not only the largest but many clusters are being formed in the system. However, both times differ only at most by a factor of 2, indicating that the estimates of the nucleation rate obtained by the MFPT method are still a very good approximation to the actual nucleation rate. Presumably, at these very large supersaturations the growth of the largest clusters quickly leads to a significant depletion of the vapor mother phase that reduces the supersaturation and prevents the formation of more clusters.

V. CONCLUSIONS

We have investigated the crossover from a nucleation-and-growth process to spinodal decomposition in a condensing LJ vapor. Using MD simulations, we are able to study the kinetics and, at the same time, also the thermodynamics of the transition by reconstructing the underlying free-energy of cluster formation.

The results show the importance of carefully distinguishing between the reaction coordinates typically chosen in theory and simulation, respectively. Very often in simulations, both MD and MC, the typical quantity being monitored is the largest cluster in the simulation, which was also primarily monitored in this work. Increasing the supersaturation in the system systematically lowers the barrier of the largest cluster $\Delta G^*_{\mathrm{larg}}$ until the point where it effectively vanishes. However, this vanishing of $\Delta G^*_{\mathrm{larg}}$ *does not* represent the occurrence of the thermodynamic spinodal. Instead, it represents the kinetic limit of the metastable mother phase, beyond which one cannot prevent the phase transition to start right away via a nucleation-and-growth mechanism. Thus, the mother phase can no longer be kept metastable, since at these conditions and just by pure equilibrium fluctuations, we may already find one cluster of critical size in the system which triggers the phase transformation. We note that this kinetic limit of metastability is system-size dependent and need not be confused with the mechanical limit of stability of the mother phase given by the thermodynamic spinodal, which lies at much higher supersaturations. Beyond this vanishing of $\Delta G^*_{\mathrm{larg}}$ and before reaching the actual thermodynamic spinodal, nucleation of the first drops occurs almost immediately and the overall rate of the phase transformation is dictated by the time it takes for these clusters to grow. Therefore, the vanishing of $\Delta G^*_{\mathrm{larg}}$ also signals the transition between a regime where the rate of the phase transformation is limited by nucleation (i.e., overcoming a barrier) and a regime where the rate is limited by how fast the drops of the new phase can grow.

We showed how the barrier for the largest cluster $\Delta G^*_{\mathrm{larg}}$ can be connected in a straightforward way to the true underlying free-energy barrier of formation of any cluster ΔG^* provided that $\Delta G^*_{\mathrm{larg}} > 0$. With this we are able to estimate the location of the spinodal by extrapolation of the data. This estimated spinodal seems to lie significantly deeper in the metastable region than the one predicted from the mean-field EOS. Visual inspection confirms the spinodal-like character of the transition as being continuous and collective throughout the entire system whereas even at very low barriers a nucleation mechanism prevails. We cross-checked the rate prediction using the CNT ansatz and prefactor by inserting directly either the reconstructed barrier heights or the Talanquer correction that is based on CNT and the estimated location of the spinodal alone. In both cases, the agreement with the measured nucleation rates is remarkable.

The nucleation barriers reconstructed in this work show good agreement with the semiempirical scaling relations suggested by McGraw and Laaksonen.[15] This is quite surprising as it suggests that the principal ansatz of CNT does work much better than expected even at such low barriers and

small cluster sizes. Moreover, it suggests that the failure of CNT cannot be related to a strong cluster-size dependence of the surface tension alone. It would be interesting to follow the same approach for different substances to see if this scaling at such small barriers is universal or just found for the simple LJ fluid.

The results of the present study also suggest that for the vapor-liquid transition in a macroscopic system, it would be very complicated, if not practically impossible, to reach the spinodal. As we increase the supersaturation the system eventually starts to phase transform right away via the nucleation mechanism long before we have actually reached the spinodal. Crystallization at low temperatures, where both nucleation and growth are expected to take place at a slower pace, would offer a better chance of reaching spinodal conditions and would thus be an ideal situation to apply the methods and insights obtained in the present study. Moreover, the understanding and control of the mechanism through which the phase transition is actually taking place might have important implications in the quality and properties of crystallized materials.

ACKNOWLEDGMENTS

This work has been partially funded by the DGCyT of the Spanish government through Grant No. FIS2005-01299, by the German DAAD through the Postdoc Fellowship D/06/49523, and by both institutions via the Acciones Integradas Hispano-Alemanas exchange program. Computing resources were provided by the University of Barcelona and the high performance cluster CLIOT of the Regional Computing Center RRZK at the University of Cologne.

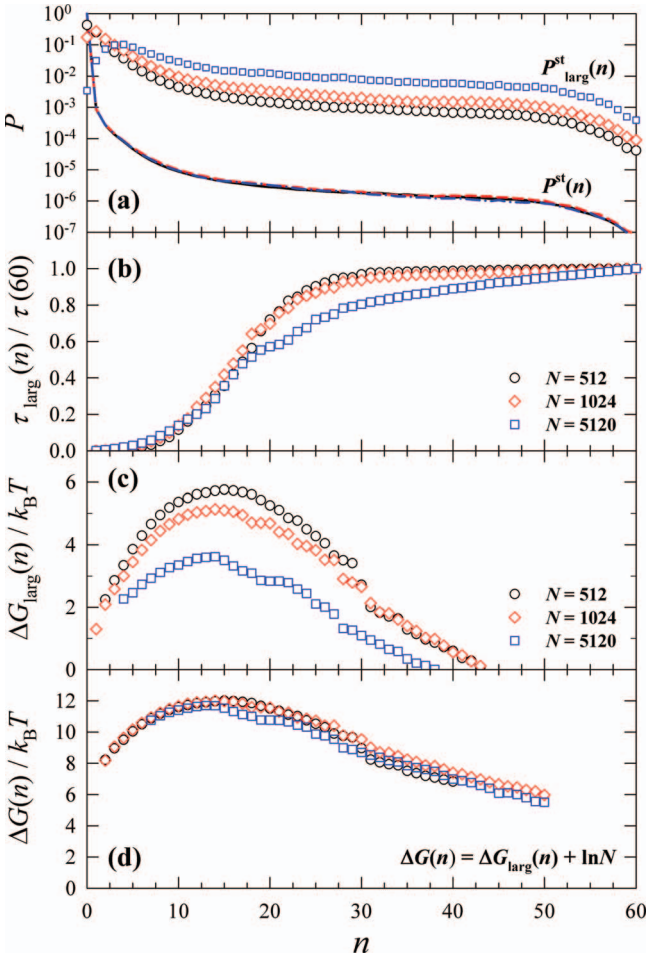

FIG. 8. Three different system sizes $N=512$, 1024, and 5120 atoms at the same supersaturation $S=12.8$. (a) Steady-state probabilities $P^{st}_{larg}(n)$ and $P^{st}(n)$. (b) Corresponding $\tau_{larg}(n)$ normalized by the value at $n=60$. (c) Reconstructed free-energy $\Delta G_{larg}(n)$. (d) Free energy of any cluster $\Delta G(n)$.

APPENDIX: CONNECTION BETWEEN THE LARGEST AND ANY CLUSTER AS THE REACTION COORDINATE

In this appendix, we discuss the connection between the relevant quantities expressed using the size of the *largest* cluster present in the system and those corresponding to the use of the size of *any* individual cluster in the system, as reaction coordinates, as well as the dependency of the results on system size. The MFPT $\tau_{larg}(n)$ and the steady-state probability $P^{st}_{larg}(n)$ of the largest cluster are related to their corresponding values for any individual cluster in a simple, although approximate, way. Gillespie[39] gave an approximate relation between the MFPT of the largest cluster $\tau_{larg}(n)$ and any individual cluster $\tau(n)$:

$$\tau_{larg}(n) \simeq \frac{\tau(n)}{N}. \tag{A1}$$

This relation holds as long as the probability distribution of first-passage times is approximately a decaying exponential in time.[39] This is indeed the case also in our simulations as long as the barrier for the largest has not yet vanished.[25] The connection between the probability distributions can be evaluated directly from the simulation: We have sampled both the steady-state probability distribution of the largest, $P^{st}_{larg}(n)$, as well as the full probability distribution of all clusters in the system, $P^{st}(n)$. It turns out that both are related in a similar fashion by

$$\frac{P^{st}_{larg}(n)}{N} \simeq P^{st}(n). \tag{A2}$$

Again, this relation holds well provided that the barrier for the largest has not yet vanished completely. These relations open up the possibility to reconstruct the free energy of interest. We can directly reconstruct the free energy of formation for the largest $\Delta G_{larg}(n)$ using the measured $\tau_{larg}(n)$ and $P^{st}_{larg}(n)$. But eventually the free energy of formation that we are interested in is that of any individual cluster $\Delta G(n)$. We can also reconstruct $\Delta G(n)$ using the full cluster-size distribution $P^{st}(n)$, which can be measured in the simulation, and the MFPT of any cluster $\tau(n)$, which cannot be evaluated easily in the simulation but which can be approximated by Eq. (A1). In both cases the reference state is taken as $n_1=1$ and $\beta\Delta G_{(larg)}(n=1)=-\ln P^{st}_{(larg)}(n=1)$. Either way, from Eqs. (3) and (4) it is straightforward to see that the resulting free

energies for the largest or any cluster are connected by the simple relation

$$\beta\Delta G(n) = \beta\Delta G_{\mathrm{larg}}(n) + \ln N, \tag{A3}$$

which was detailed in Eq. (12) for the top of the barrier.

The validity of this relation can be verified by repeating the simulations at the same supersaturation (density) but for different system sizes (different values of N). One important aspect of the quantities expressed in terms of the largest cluster is their system-size dependence. In contrast, the underlying quantities of interest expressed in terms of any individual cluster should *not* depend on how many molecules we use in the simulation. Figure 8 shows the measured steady-state probabilities, the MFPT $\tau_{\mathrm{larg}}(n)$, and the reconstructed free energies $\Delta G_{\mathrm{larg}}(n)$ and $\Delta G(n)$ for the system sizes of $N=512$, 1024, and 5120 but the same supersaturation $S=12.8$. The measured steady-state probability of the largest $P^{\mathrm{st}}_{\mathrm{larg}}(n)$ changes with system size as expected, but the one for any cluster $P^{\mathrm{st}}(n)$ stays the same regardless of system size. The MFPT, normalized by the value of $\tau_{\mathrm{larg}}(n=60)$, shows a similar trend as the one shown in Fig. 1. But note that here it is only the size of the system that changes and not the supersaturation. The vanishing of the plateau in the MFPT curve toward larger system sizes already signals that the barrier for the largest $\Delta G_{\mathrm{larg}}(n)$ diminishes. This is indeed the case for the BRs plotted in Fig. 8(c): The larger the total number of molecules N in the simulation, the smaller is the barrier for the largest despite the fact that the supersaturation is the same. However, using Eq. (A3) to correct for the size dependence of $\Delta G_{\mathrm{larg}}(n)$ we can verify that the curves for all different system sizes nicely collapse into a single curve for the work of formation of any individual cluster $\Delta G(n)$, as shown in Fig. 8(d). Indeed, in comparison with our reference system of 512 argon atoms $\Delta G_{\mathrm{larg}}(n)$ gets smaller by almost exactly the expected values of $\ln(1024/512) \approx 0.7 k_{\mathrm{B}}T$ for the system with 1024 atoms and by $\ln(5120/512) \approx 2.3 k_{\mathrm{B}}T$.

[1] F. F. Abraham, S. W. Koch, and R. C. Desai, Phys. Rev. Lett. **49**, 923 (1982).
[2] D. Stauffer, A. Coniglio, and D. W. Heermann, Phys. Rev. Lett. **49**, 1299 (1982).
[3] W. Klein and C. Unger, Phys. Rev. B **28**, 445 (1983).
[4] K. Binder, Phys. Rev. A **29**, 341 (1984).
[5] W. Klein and F. Leyvraz, Phys. Rev. Lett. **57**, 2845 (1986).
[6] P. G. Debenedetti, *Metastable Liquids: Concepts and Principles* (Princeton University Press, Princeton, 1996).
[7] S. Auer and D. Frenkel, Nature (London) **413**, 711 (2001).
[8] G. Wilemski and J. S. Li, J. Chem. Phys. **121**, 7821 (2004).
[9] F. Trudu, D. Donadio, and M. Parrinello, Phys. Rev. Lett. **97**, 105701 (2006).
[10] W. Klein, H. Gould, N. Gulbahce, J. B. Rundle, and K. Tiampo, Phys. Rev. E **75**, 031114 (2007).
[11] P. Bhimalapuram, S. Chakrabarty, and B. Bagchi, Phys. Rev. Lett. **98**, 206104 (2007).
[12] L. Maibaum, Phys. Rev. Lett. **101**, 019601 (2008).
[13] L. Maibaum, Phys. Rev. Lett. **101**, 256102 (2008).
[14] V. K. Shen and J. R. Errington, J. Phys. Chem. B **108**, 19595 (2004).
[15] R. McGraw and A. Laaksonen, Phys. Rev. Lett. **76**, 2754 (1996).
[16] M. P. Allen and D. J. Tildesley, *Computer Simulation of Liquids* (Oxford University Press, Oxford, 1989).
[17] D. Frenkel and B. Smit, *Understanding Molecular Simulation* (Academic, San Diego, 2002).
[18] J. Wedekind, D. Reguera, and R. Strey, J. Chem. Phys. **125**, 214505 (2006).
[19] J. Wedekind, D. Reguera, and R. Strey, J. Chem. Phys. **127**, 064501 (2007).
[20] V. G. Baidakov, S. P. Protsenko, Z. R. Kozlova, and G. G. Chernykh, J. Chem. Phys. **126**, 214505 (2007).
[21] P. R. ten Wolde and D. Frenkel, J. Chem. Phys. **109**, 9901 (1998).
[22] J. Wedekind and D. Reguera, J. Chem. Phys. **127**, 154516 (2007).
[23] J. L. Katz and M. D. Donohue, in *Advances in Chemical Physics*, edited by I. Prigogine and S. A. Rice (Wiley, New York, 1979), p. 137.
[24] J. Wedekind, R. Strey, and D. Reguera, J. Chem. Phys. **126**, 134103 (2007).
[25] G. Chkonia, J. Wölk, R. Strey, J. Wedekind, and D. Reguera, J. Chem. Phys. **130**, 064505 (2009).
[26] P. Hänggi, P. Talkner, and M. Borkovec, Rev. Mod. Phys. **62**, 251 (1990).
[27] J. Frenkel, *Kinetic Theory of Liquids* (Clarendon, Oxford, 1946).
[28] J. Wedekind and D. Reguera, J. Phys. Chem. B **112**, 11060 (2008).
[29] W. H. Press, S. A. Teukolsky, W. T. Vetterling, and B. P. Flannery, *Numerical Recipes 3rd Edition: The Art of Scientific Computing* (Cambridge University Press, Cambridge, 2007).
[30] D. Kashchiev, J. Chem. Phys. **76**, 5098 (1982).
[31] D. W. Oxtoby and D. Kashchiev, J. Chem. Phys. **100**, 7665 (1994).
[32] R. K. Bowles, D. Reguera, Y. Djikaev, and H. Reiss, J. Chem. Phys. **115**, 1853 (2001).
[33] H. Wang, H. Gould, and W. Klein, Phys. Rev. E **76**, 031604 (2007).
[34] E. Mendez-Villuendas, I. Saika-Voivod, and R. K. Bowles, J. Chem. Phys. **127**, 154703 (2007).
[35] J. K. Johnson, J. A. Zollweg, and K. E. Gubbins, Mol. Phys. **78**, 591 (1993).
[36] B. Smit, J. Chem. Phys. **96**, 8639 (1992).
[37] V. Talanquer, J. Chem. Phys. **106**, 9957 (1997).
[38] A. P. Grinin, A. K. Shchekin, F. M. Gruni, E. A. Grinina, and H. Reiss, J. Chem. Phys. **121**, 387 (2004).
[39] D. T. Gillespie, J. Chem. Phys. **74**, 661 (1981).